Visualization of Wing Tip Vortices in Accelerating and Steady Flow

P. Freymuth,* F. Finaish,† and W. Bank‡
University of Colorado, Boulder, Colorado

Introduction

FOR flow around a periodically pitching rectangular wing, Adler and Luttges[1] estimated the influence of the tip vortex to extend one chordlength inboard from the tip by using a smoke wire technique. No further structural detail for this tip vortex is known. Francis and Kennedy[2] noted that even for steady flow little is known about the vortical structure near the tip of a rectangular wing.

Flow visualization seems to be the best approach to obtain clues about complex vortical structures. We have used a streakline method[3] to visualize complex two-[4] and three-dimensional[5] vortical structures over an airfoil. This method can be further extended to visualize wing tip vortices in unsteady and steady flows, as will be demonstrated in this paper.

Experimental Description

Our wind tunnel and basic visualization methods have been described before.[3-5] A wind tunnel with horizontal test section 91×91 cm in height and width can be driven in either a mode of constant acceleration starting from rest or in a steady-speed mode. A rectangular wing with NACA 0015 profile and with a chord length $c = 15.2$ cm protrudes 45 cm into the tunnel. The wing is fastened in a round holder or turntable on the top wall of the tunnel and can be adjusted to an arbitrary angle of attack.

Liquid titanium tetrachloride is administered by means of a brass pipette through appropriate holes in the turntable, either near the leading or trailing edge of the wing. This liquid runs down along the leading or trailing edge to the wing tip and forms a smoke-producing liquid film. The smoke envelopes the wing and marks the vortical structures. The smoke is floodlit from the top and is photographed through the transparent front wall of the test section from which the suction side of the wing is visible. Movie sequences of the streakline patterns were taken with a Bolex camera at a rate of 64 frames/s and at 1/400 s exposure time.

Visualization in Accelerating Flow Starting from Rest

As has been stated by us previously,[4] the flow acceleration in the tunnel is $a = 2.4$ m/s^2 after flow startup. A wing with chord length $c = 15.2$ cm was used, yielding a Reynolds number $R = a^{1/2}c^{3/2}\nu^{-1} = 5200$, where $\nu = 0.18$ cm^2/s was the kinematic viscosity in air.

Figure 1 shows a sequence with view onto the suction side of the wing, at an angle of attack $\alpha = 10$ deg. In all sequences, consecutive frames are ordered into columns from top to bottom and then across columns from left to right. The flow is always from left to right. The time from flow startup to the first frame shown is $t_1 = 47/64$ s, the time between frame shown is $\Delta t = 4/64$ s for all sequences, and the frame height corresponds to an actual height of $h = 16.4$ cm.

Smoke-generating liquid was released along the leading edge of the wing, marked by the left arrow on top of the first frame. The trailing edge is covered with smoke and its location is marked by the right arrow at top of the first frame. The tip location can be seen as a horizontal boundary of illumination

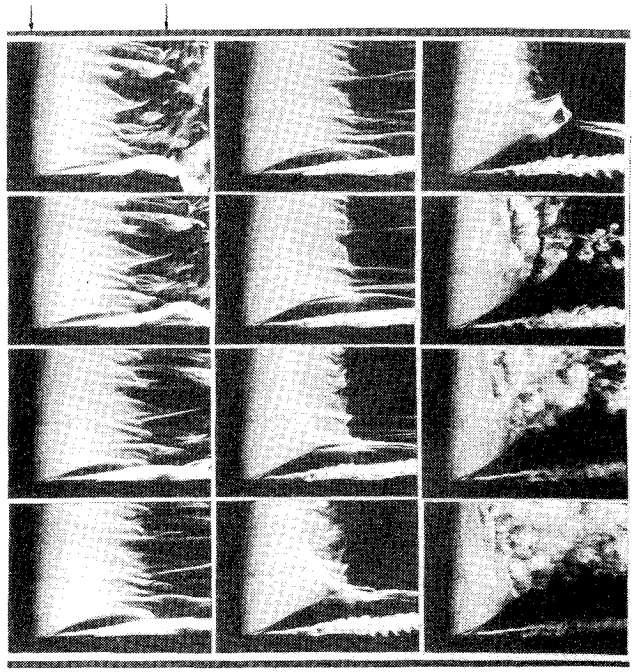

Fig. 1 Sequence with view onto the suction side of the wing ($\alpha = 10$ deg, $t_1 = 47/64$ s, $\Delta t = 4/64$ s, frame height $h = 16.4$ cm).

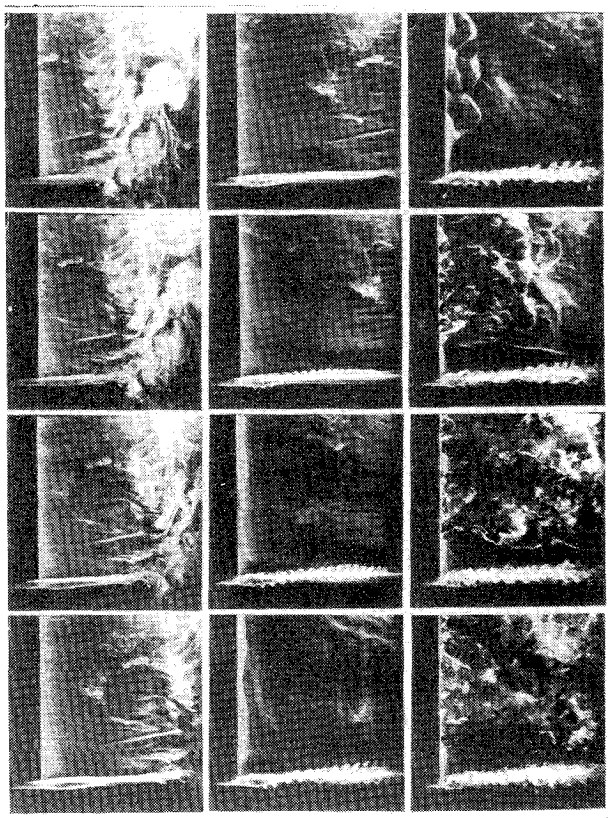

Fig. 2 Sequence with view downstream of the trailing edge ($\alpha = 10$ deg, $t_1 = 30/64$ s, $\Delta t = 4/64$ s, $h = 38.5$ cm).

Received Nov. 17, 1985; presented as Paper 86-1096 at the AIAA/ASME 4th Fluid Mechanics, Plasma Dynamics and Lasers Conference, Atlanta, GA, May 12-14, 1986.

*Professor, Department of Aerospace Engineering Sciences.
†Graduate Student, Department of Aerospace Engineering Sciences.
‡Electronics Engineer, Department of Aerospace Engineering Sciences.

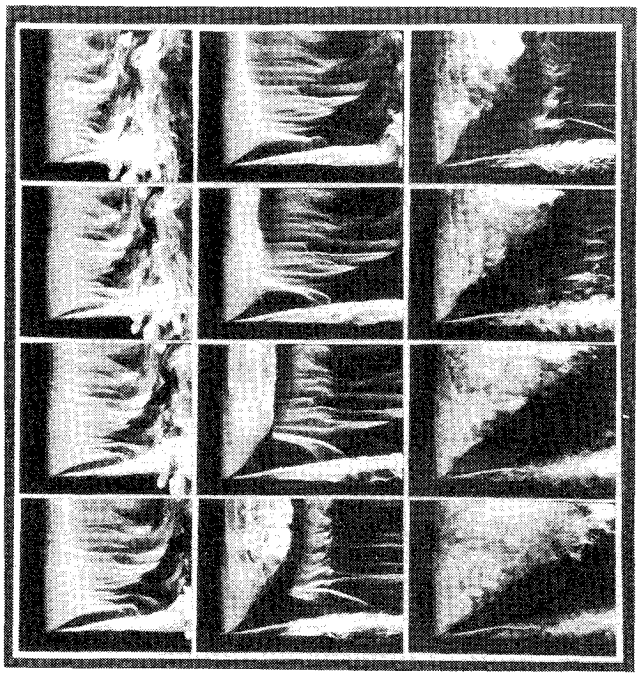

Fig. 3 Sequence with view onto the suction side of the wing ($\alpha = 20$ deg, $t_1 = 25/64$ s, $\Delta t = 4/64$ s, $h = 16.4$ cm).

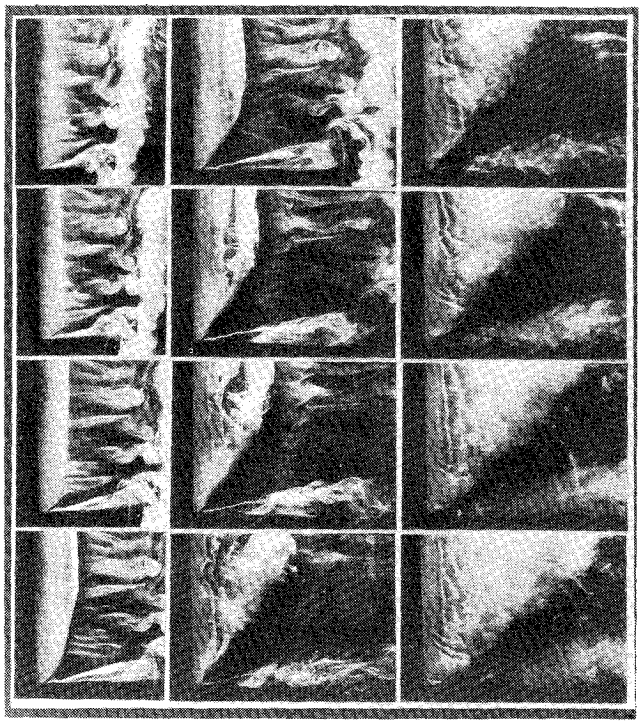

Fig. 5 Sequence with view onto the suction side of the wing ($\alpha = 30$ deg, $t_1 = 25/64$ s, $\Delta t = 4/64$ s, $h = 18.6$ cm).

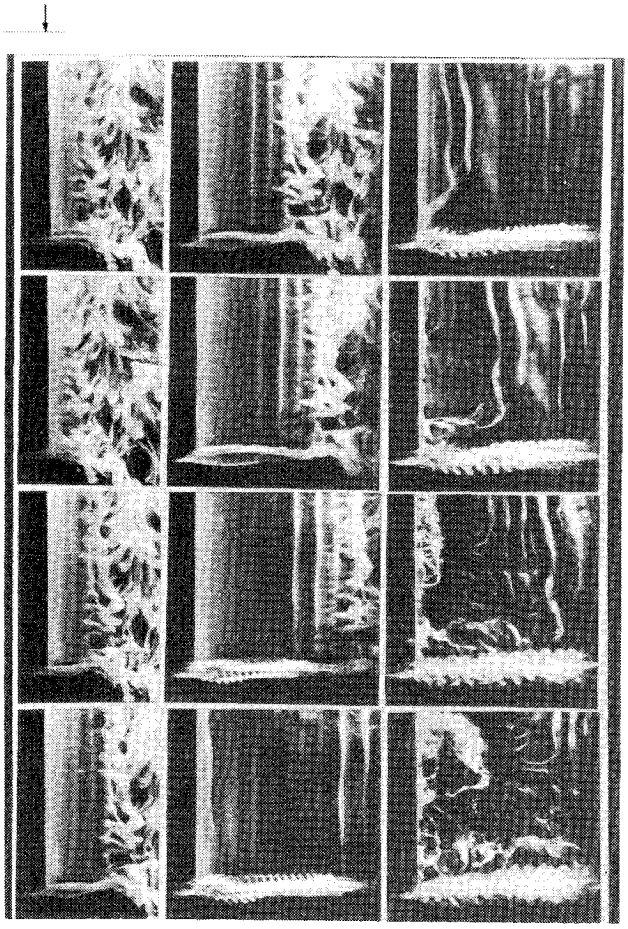

Fig. 4 Sequence with view downstream of the trailing edge ($\alpha = 20$ deg, $t_1 = 17/64$ s, $\Delta t = 4/64$ s, $h = 38.5$ cm).

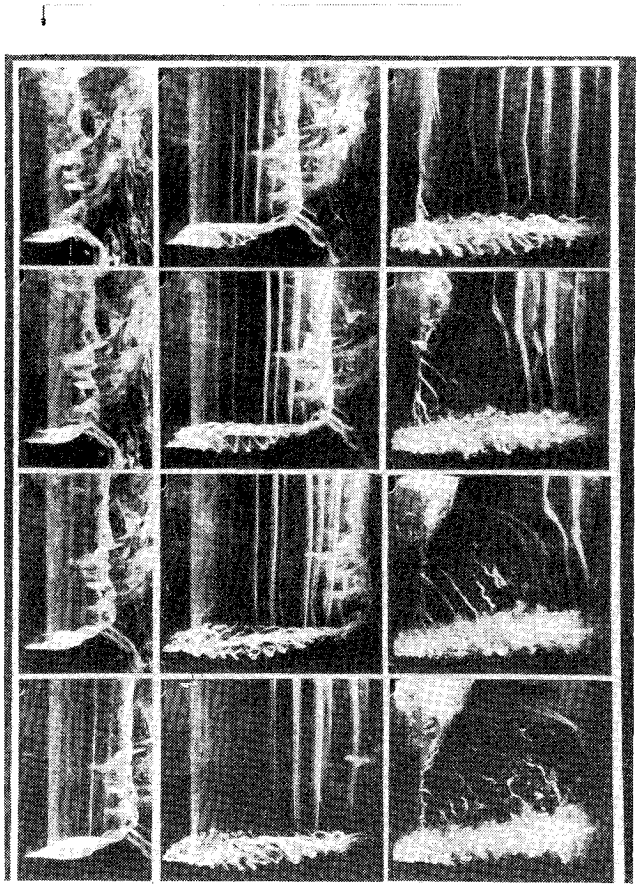

Fig. 6 Sequence with view downstream of the trailing edge ($\alpha = 30$ deg, $t_1 = 18/64$ s, $\Delta t = 4/64$ s, frame height $h = 38.5$ cm).

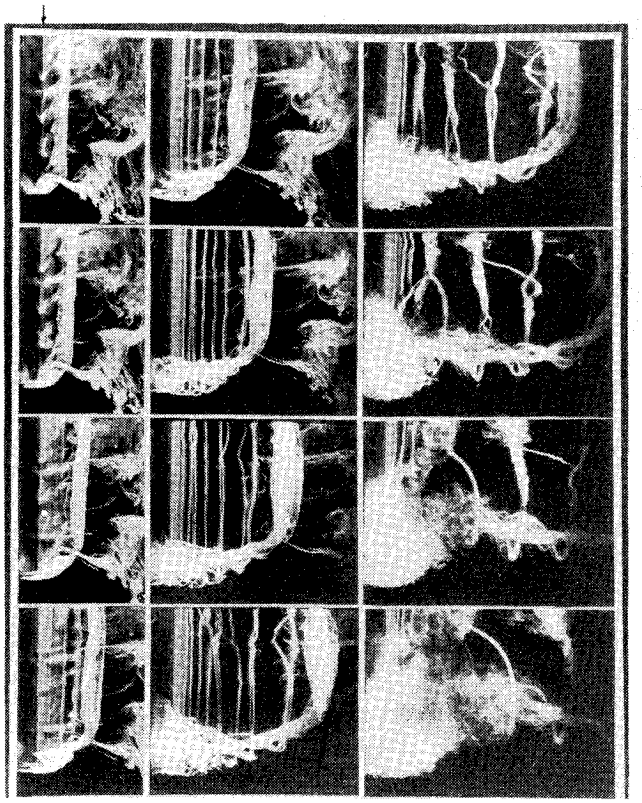

Fig. 7 Sequence with view downstream of the trailing edge ($\alpha = 60$ deg, $t_1 = 19/64$ s, $\Delta t = 4/64$ s, $h = 38.5$ cm).

near the bottom of each movie frame. A nearly horizontal wing tip vortex can be seen with a conical shape, its apex pointing to the front corner of the wing tip. This vortex is separated from the smoke sheet over the wing. In column 3, leading edge vortices form over and downstream of the wing surface. These vortices seem to end at the front corner, but this can be seen better in subsequent figures taken at higher angles of attack. The leading-edge vortices quickly become turbulent, as is shown by the diffuseness of the smoke in the last few frames.

To visualize the wing tip vortex further downstream and to show its connection to the vortex sheet shed from the trailing edge, smoke-generating liquid was introduced from the pressure side and was allowed to run down the trailing edge of the wing. In Fig. 2, the dark trailing edge can be seen as marked by an arrow on top of the first frame. An illuminated smoke sheet leaves the trailing edge, which at its lower boundary connects to the horizontal wing tip vortex. This vortex develops a filamentary structure whose significance can be judged better in subsequent visualizations at higher angles of attack.

Figure 3 shows development on top of the wing at an angle of attack $\alpha = 20$ deg. Again, the development of the nearly horizontal wing tip vortex in the form of a cone is easily recognized. The vertical leading-edge vortices develop earlier and turn left toward the front corner, where they also seem to end in a cone. As seen in column 3, turbulence, recognizable by the diffuseness of the smoke, sets in strongly.

Figure 4 shows the corresponding development downstream of the trailing edge. The trailing-edge vortex sheet decays into a series of discrete starting vortices visibile as light vertical filaments in column 2. These lines wind up as filaments of the horizontal wing tip vortex, which explains why the wing tip vortex has a filamentary structure. In column 3, the patterns become more chaotic, but it can be seen that the vortices leaving the trailing edge at this stage of development do not wind up in the tip vortex, but turn toward the back corner of the wing tip (frames 1 and 2 in column 3). This represents an added complication in the late stages of development.

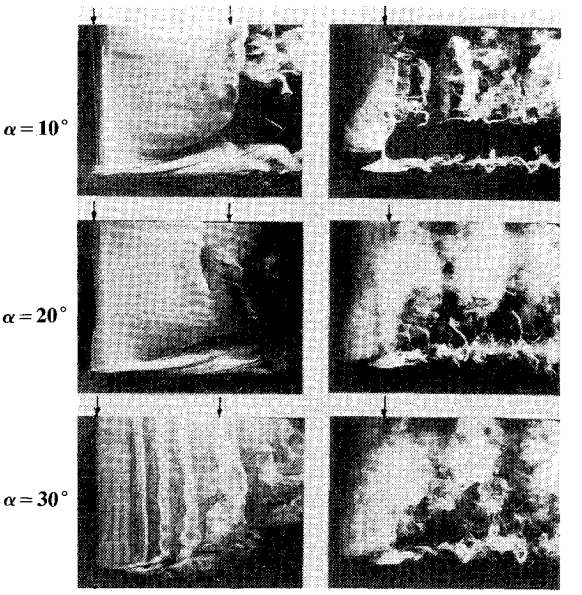

Fig. 8 Single frames in steady flow at $Re = 5200$, angles as indicated in the figure (left to column: view at the suction side of the wing, $h = 18.5$ cm; right column: view downstream of the trailing edge, $h = 38.5$ cm).

Figure 5 shows the development on top of the wing at an angle of attack $\alpha = 30$ deg. The development of the conical pair of vortices near the front corner shows up quite clearly, a structure that persists into the turbulent regime.

The corresponding development behind the trailing edge shown in Fig. 6 illustrates very clearly how the trailing-edge starting vortices feed the filmantary structure of the wing tip vortex. Again, at the later stage in column 3, this direct feeding ceases and newly generated trailing-edge vortices seem to converge on the trailing edge somewhat above the wing tip vortex.

Figure 7 is included to convey how dramatic the developments become behind the trailing edge at very high angles of attack, in this case $\alpha = 60$ deg. The trailing-edge starting vortices that join the wing tip vortex go through partial pairing processes prior to their turbulent breakdown.

Visualization in Steady Flow

We also visualized smoke patterns over the wing in slow steady flow. The speed was $U_0 = 61$ cm/s, which resulted in a Reynolds number of $Re = U_0 c \nu^{-1} = 5200$. The same wing was used at angles of attack $\alpha = 10$, 20 and 30 deg. The smoke patterns of interest were more static in steady flow and, therefore, for a given angle, only one frame is shown for the patterns near the leading edge and one for those behind the trailing edge. All of these frames have been mounted and identified in Fig. 8. First, consider the visualization on top of the wing (left column). At all three angles of attack, a tip vortex and its separation from the suction side vortex sheet is discernible as before. However, the separation of these features is much narrower than in the accelerating flow starting from rest. Periodic shedding of leading-edge vortices can be seen, in particular at $\alpha = 30$ deg.

The right column shows that visualization behind the trailing edge at the three angles of attack. Trailing-edge vortices and the tip vortex seem not to connect to each other at $\alpha = 10$ deg and connect only sporadically at the higher angles. This is similar to the late stages of development downstream of the trailing edge in accelerating flow.

Conclusion

The wing tip vortex system in a starting flow has been visualized at a Reynolds numer of 5200. A similar structure was found in steady flow. The influence of the vortex structure on Reynolds number, the dependence on the profile and

tip geometry, and the applicability to other unsteady flows remain for future investigation.

References

[1]Adler, J.N. and Luttges, M.W., "Three-Dimensionality in Unsteady Flow about a Wing," AIAA Paper 85-0132, 1985.

[2]Frances, M.S. and Kennedy, D.A., "Formation of a Trailing Vortex," *Journal of Aircraft*, Vol. 16, March 1979, pp. 148-154.

[3]Freymuth, P., Bank, W., and Palmer, M., "Use of Titanium Tetrachloride for Visualization of Accerlerating Flow Around Airfoils," *Flow Visualization,* Vol. III, Hemisphere Press, New York, 1985, pp. 99-105.

[4]Freymuth, P., Bank, W., and Palmer, W. "Visualization of Accelerating Flow Around an Airfoil at High Angles of Attack," *Zeitschrift fuer Flugwissenschaften und Weltraumforschung*, Vol. 7, 1983, pp. 392-400.

[5]Freymuth, P., Finaish, F., and Bank, W. "Three-Dimensional Vortex Patterns in a Starting Flow," *Journal of Fluid Mechanics,* Vol. 161., 1985, pp. 239-248.

Airplane Flight Through Wind-Shear Turbulence

George Treviño*
Michigan Technological University
Houghton, Michigan

Nomenclature

a,b	= time-dependent parameters defining anisotropic effects on two-point velocity correlation structure
A,B,C,D	= arbitrary functions in the invariant algebraic representation of correlation tensor(s)
$C_{ij}(r)$	= two-point velocity correlation tensor for anisotropic turbulence
f,g	= longitudinal, transverse correlation functions for isotropic turbulence
$K(t)$	= variable defined in Eq. (3); $K(t)>0$ for all t
L	= transverse correlation length for anisotropic turbulent downwash
M	= slope of mean-flow shear
r	= magnitude of $\boldsymbol{r}$, i.e., $r=\|\boldsymbol{r}\|$
$\boldsymbol{r}$	= separation vector for turbulence velocity correlations
$R_{ij}(r)$	= two-point velocity correlation tensor for isotropic turbulence
$S_{ijl}(r)$	= two-point "turbulence self-interaction" tensor
$\boldsymbol{u}$	= turbulence velocity = (u,v,w)
$\bar{U}$	= mean-flow velocity = $(\bar{U},0,0)$
α	= glide-slope angle for aircraft landing (or takeoff)
λ	= unit vector defining preferred direction of turbulence anisotropy
Λ	= longitudinal correlation length for isotropic turbulence
$\Delta\Lambda$	= change in correlation length due to turbulence anisotropy
ξ	= scalar variable defined for anisotropic turbulence, $=\lambda\cdot\boldsymbol{r}$
σ	= turbulence intensity

Received March 15, 1986.

*Associate Professor of Engineering Mechanics. Member AIAA.

Introduction

In a recent Note[1] it was established why traditional schemes (see Ref. 2 and references cited therein) for simulating air turbulence typically lead to "unacceptable" results. In particular, it was shown that the historical Gaussian time-history approach as well as the modern modified Gaussian approach do not at all model the nonlinear convective effect which is eminently characteristic of hydrodynamic turbulence. In fact, both approaches completely disdain this phenomenon and proceed as though the turbulence and mean-flow velocities, $\boldsymbol{u}$ and $\bar{U}$, respectively, can be linearly superimposed with no related interplay. Note that convection is analogous to skewness in the probability density function (pdf) of the turbulence, and any pdf that is symmetric about $\boldsymbol{u}\equiv 0$ automatically has zero skewness.

In this Note the effect of *mean-flow shear* ("wind shear") on the turbulence structure is examined. Shear is the description given to a mean flow, which is spatially nonconstant, say $\bar{U}\sim\bar{U}(x)$, and its most pronounced effect is the strong anisotropy it unfortunately generates. Shear is encountered by an airfract in the atmospheric boundary-layer when the aircraft is usually in the takeoff or landing mode. It may also be encountered at high altitudes; however, these encounters, from the viewpoint of aviation safety, are potentially not as hazardous. In the sequel it is shown that as an airplane encounters a "microburst" even a small amount of anisotropy produces a significant time variation in the sensed magnitude of the *integral scale*—a measure of the degree of "randomness' in turbulence; "large" integral scale ~ moderately random turbulence while "small" integral scale ~ highly random turbulence.

Anisotropy for Flight Simulation

The two-point velocity correlation for anisotropic turbulence is[3]

$$\langle u_i(x)u_j(x+r)\rangle = C_{ij}(r) = Ar_ir_j + B\delta_{ij}$$

$$+ C\lambda_i\lambda_j + D(\lambda_i r_j + r_i\lambda_j)$$

where A, B, C, and D are arbitrary functions of $r^2=\boldsymbol{r}\cdot\boldsymbol{r}$ and $\xi=\lambda\cdot\boldsymbol{r}=r\cos\theta$ (also t, but this dependence is suppressed here for convenience). It can be readily shown[3] that A, B, and C are even functions of both r and ξ, but D, on the other hand, is an odd function of ξ. For boundary-layer turbulence, the unit vector λ can be assumed to have components $\lambda=(0,0,1)$, indicating that the vertical (z) direction is the proverbial "preferred direction of the flow." Note that this expression for $C_{ij}(r)$ is different from that for *isotropic* turbulence, namely, $R_{ij}(r)=Ar_ir_j+B\delta_{ij}$, where $A\sim A(r$ only$)=\sigma^2(f-g)/r^2$ and $B\approx B(r$ only$)=\sigma^2 g$; consistent with isotropic theory, $f\sim$ *longitudinal* correlation function, $g\sim$ *transverse* correlation, and $\sigma\sim$ *intensity*. When an airplane is either taking off or landing, its flight path is generally such that $\xi=\lambda\cdot\boldsymbol{r}=r\sin\alpha\simeq r\alpha$ (see Fig. 1); therefore, for the considered simulation purpose, the preceding functions A, B, C, and D can be roughly approximated as $A(r^2,\xi)\simeq A(r^2,0)$, $B(r^2,\xi)\simeq B(r^2,0)$, $C(r^2,\xi)\simeq C(r^2,0)$, and $D(r^2,\xi)\simeq D(r^2,0)\equiv 0$. Accordingly, the corresponding turbulence correlations are

$$C_{11}(r) = r^2A + B \simeq \sigma^2 f(r)$$

$$C_{22}(r) = B \simeq \sigma^2 g(r)$$

$$C_{33}(r) = \alpha^2 r^2 A + B + C \simeq B + C \neq \sigma^2 g(r)$$

$$C_{13}(r) = \alpha r^2 A = \alpha\sigma^2\{f(r) - g(r)\}$$

where $\boldsymbol{r}=(r_x,0,r_z)\simeq(r,0,\alpha r)$; note that A and B here are identical to the isotropic case, namely, $A=\sigma^2(f-g)/r^2$ and